ROYAL SOCIETY
OF CHEMISTRY

COMMUNICATION

Check for updates

An artificial protein-probe hybrid as a responsive probe for ratiometric detection and imaging of hydrogen peroxide in cells†

Xing Zhang,[ab] Youxin Fu, [ID][b] Guangren Qian, [ID] *[a] Run Zhang [ID][b] and Zhi Ping Xu [ID] *[b]

An artificial protein-probe hybrid, Cm–Np-B@BSA, was prepared *via* host–guest interactions between hydrogen peroxide (H_2O_2)-responsive Cm–Np-B molecule and bovine serum albumin (BSA). The Cm–Np-B@BSA probe exhibited high sensitivity and selectivity towards H_2O_2 under physiological conditions and had excellent biocompatibility, allowing for sensitive ratiometric detection and imaging of endogenous H_2O_2 in live cells.

Fluorescent protein has emerged as an attractive platform in designing responsive probes for real-time detection and monitoring of specific biomarkers in biological systems.[1–3] In the past few decades, many efforts have been made to produce genetically encoded fluorescent protein probes to respond to biomarkers and investigate their applications in biology and biomedicine.[4–7] Despite the advantages of fluorescent protein probes in biosensing and bioimaging (such as excellent biocompatibility), only a limited number of responsive fluorescent protein probes have been reported.[4,8,9] This is mainly because the tedious procedure for fluorescent protein production restricts their expression on a large scale.

In order to overcome this limitation, several artificial protein-probe hybrids were made by integrating a fluorophore (*e.g.* organic fluorescent dye, luminescent metal complex, or quantum dot) with a suitable protein *via* supermolecular and host–guest interactions, or chemical conjugations.[10–13] This kind of hybrid provides an alternative scaffold for designing responsive fluorescent protein-probe hybrids for biological applications.[10,12] Incorporating various fluorophores, especially fluorescent organic dyes, into proteins to yield artificial protein-probe hybrids enhances the biocompatibility and bioavailability of fluorescent dyes. More importantly, the artificial hybrid enables biomarker detection in aqueous solutions and physiological

conditions without fluorescence quenching caused by dye molecule aggregation.[14,15] For example, coumarin was loaded into the cavities of bovine serum albumin (BSA),[16–18] and emitted characteristic fluorescence that was quenched in its aggregation state in water. With interactions between the fluorophore and protein, several fluorescent dyes, including coumarin, have been reported for protein detection in aqueous solutions.[12,13,19–21] In this work, we expanded this idea and developed an artificial protein-probe hybrid specific for hydrogen peroxide (H_2O_2) detection, and also highlighted the strategy of developing artificial protein-probe hybrids beyond the aforementioned protein detection.

H_2O_2, produced during mitochondrial respiration, is one of the most important reactive oxygen species (ROS) in biological systems.[22–28] Endogenous H_2O_2 is the most stable ROS, having the lowest reactivity and the highest intracellular concentration ($\sim 10^{-8}$–10^{-4} M).[29] In living organisms, this biomolecule serves as an essential biomarker in regulating a wide variety of physiological events, such as activation of diverse signalling pathways to stimulate cell proliferation, differentiation, migration, and apoptosis.[29–32] The role of H_2O_2 in biological systems is concentration-dependent.[33] It is, therefore, highly demanded to develop suitable responsive fluorescence probes for H_2O_2 detection in live cells for a better understanding of H_2O_2-mediated biofunctions.[34]

Different from previously reported molecule probes for H_2O_2 detection, this communication presents a biocompatible responsive protein-probe hybrid for ratiometric detection of H_2O_2 in aqueous solutions and living systems through a simple one-step self-assembly of organic dye **Cm–Np-B** with BSA. As shown in Scheme 1, the dye (**Cm–Np-B**) was designed based on the elegant modulation of the intramolecular charge transfer (ICT) and the Förster resonance energy transfer (FRET).[35–37] The emission of energy transfer (ET) donor, *i.e.* coumarin (**Cm**, blue channel) can be activated after loading into the cavity of BSA through host–guest interactions in PBS buffer. Within the BSA system (**Cm–Np-B@BSA**), the emission of the ET acceptor, *i.e.* naphthalimide (**Np**, green channel), is quenched due to the inability of

[a] School of Environmental Science and Chemical Engineering, Shanghai University, Shanghai 200444, China. E-mail: grqian@shu.edu.cn

[b] Australian Institute for Bioengineering and Nanotechnology, The University of Queensland, St Lucia, QLD 4072, Australia. E-mail: gordonxu@uq.edu.au

† Electronic supplementary information (ESI) available. See DOI: 10.1039/d0tb00856g
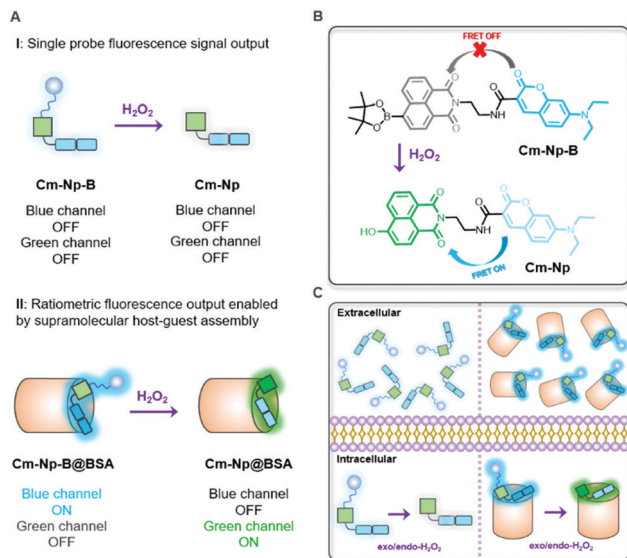
Scheme 1 Design of an artificial protein-probe hybrid (**Cm–Np-B@BSA**) for responsive H_2O_2 detection. (A) ON–OFF non-response of molecular probe (i) and response of BSA-probe (ii); (B) ON–OFF responsive mechanism; (C) cellular responses for H_2O_2 detection.

the ICT process. Through an H_2O_2-triggered reaction to cleave boronate group,[38] the "donor-π-acceptor (D-π-A)" hydroxyl-Np derivative (**Cm–Np@BSA**) is generated and thus the emission of Np is switched "ON". Moreover, the formation of **Cm–Np@BSA** also enables FRET from **Cm** to **Np**, allowing ratiometric fluorescence detection and bioimaging of H_2O_2 with a blue-to-green fluorescence colour change.

The fluorescent dye, **Cm–Np-B**, was synthesized in a four-step procedure with a reasonable yield (Scheme S1, ESI†), and the chemical structures of **Cm–Np-B** and the intermediates were identified with NMR and ESI-MS (Fig. S1–S5, ESI†). Then the protein-probe hybrid (**Cm–Np-B@BSA**) was made through simply mixing the probe and BSA in PBS buffer (Page S6, ESI†).

The blue channel activation of **Cm–Np-B@BSA** was first evaluated by UV-vis absorption and fluorescence spectra. As shown in Fig. 1A, **Cm–Np-B** was essentially non-fluorescent in both the blue and green channels in PBS buffer (pH 7.4, black dashed curve), largely attributed to the aggregation-caused
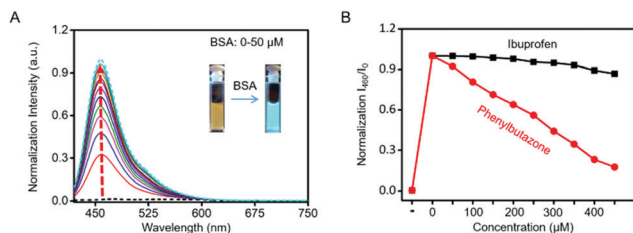

Fig. 1 Formation of **Cm–Np-B@BSA** and its fluorescence. (A) fluorescence spectra of **Cm–Np-B** (5 µM) at different concentrations of BSA (0–50 µM); (B) fluorescence intensity changes in **Cm–Np-B@BSA** (5/50 µM, means 5 µM probe with 50 µM protein) with the concentration of ibuprofen (black solid line) and phenylbutazone (red solid line) increasing from 0 to 450 µM in PBS buffer (0.5% DMSO (v/v), pH 7.4; excitation wavelength: 410 nm).

quenching (ACQ).[39] In sharp contrast, the fluorescence intensity was gradually increased upon mixing with more BSA (from 0 to 50 µM) and maximum enhancement of emission intensity (>145-fold) at 460 nm was achieved at 50 µM of BSA. Simultaneously, a new peak in the UV-vis absorption spectrum at 280 nm was observed, which is attributed to the characteristic absorbance of BSA (Fig. S6, ESI†). Similarly, **Cm–Np-B** is also responsive to human serum albumin (HSA). As shown in Fig. S7 (ESI†), the fluorescence intensity gradually increased upon mixing with more HSA (from 0 to 50 µM), presumably due to the similar 3D structure, chemical composition, and biological functions of these two albumins.

Dynamic light scattering (DLS) analysis showed a large size of molecule probe **Cm–Np-B** (600–700 nm) in PBS buffer (Fig. S8, ESI†), due to aggregation of **Cm–Np-B** molecules in PBS. Upon assembling **Cm–Np-B** with BSA, the hydrodynamic diameter of the **Cm–Np-B@BSA** hybrids was 17.8 ± 1.3 nm, slightly larger than that of BSA (13.0 ± 0.3 nm). The size increase and disappearance of **Cm–Np-B** aggregates together confirm formation of the guest–host complexes (**Cm–Np-B@BSA**) via binding **Cm–Np-B** into the hydrophobic pocket of BSA with a slightly big volume.

As shown in Fig. 1A, the emission intensity of **Cm–Np-B** dye was BSA-concentration dependent. Fluorescence Job's plot analysis showed a maximum intensity at the molecular fraction of 0.5 (Fig. S9, ESI†), indicating the 1 : 1 binding stoichiometry between **Cm–Np-B** and BSA. **Cm–Np-B** is thus located only at one binding site of BSA. Previous reports have shown that most small hydrophobic molecules are wrapped into the hydrophobic pockets of BSA, i.e. site I and site II.[40–42] Phenylbutazone and ibuprofen are known to bind site I and site II of BSA, respectively. In order to determine the binding site, a competitive assay was carried out to displace **Cm–Np-B** from BSA using these two albumin-binding molecules. As shown in Fig. 1B, the intensity of blue emission at 460 nm was decreased upon adding phenylbutazone, while adding ibuprofen caused a negligible change in the fluorescence intensity. The selective replacement of **Cm–Np-B** by phenylbutazone suggests that the preferred binding site of **Cm–Np-B** is site I of BSA. In addition, the blue channel emission of the probe largely decreased upon adding trypsin, suggesting the release of **Cm–Np-B** into PBS buffer and subsequent aggregation after BSA degradation (Fig. S10, ESI†).

To test the fluorescence response of **Cm–Np-B@BSA** to H_2O_2, **Cm–Np-B@BSA** in PBS buffer was treated with H_2O_2 at different concentrations and the changes in UV-vis absorbance and fluorescence spectra were recorded. As shown in Fig. S11A (ESI†), the absorbance at $\lambda_{abs} = 350$ nm was gradually decreased and the maximum absorbance band at $\lambda_{abs} = 430$ nm was gradually intensified upon the addition of H_2O_2 (0–200 µM). The change of UV-vis absorption spectra is ascribed to the ICT feature in **Cm–Np** dye due to the transformation of **Cm–Np-B@BSA** to **Cm–Np@BSA** (Scheme 1). Clearly, the UV-vis absorption spectral change in **Cm–Np-B@BSA** towards H_2O_2 was more sensitive than that of **Cm–Np-B** (Fig. S11B, ESI†), suggesting the higher sensitivity of the artificially devised fluorescent protein-probe hybrid.

As shown in Fig. 2A, **Cm–Np-B@BSA** exhibited a blue emission band from the coumarin donor ($\lambda_{ex} = 410$ nm, $\lambda_{em} = 460$ nm) in the

absence of H_2O_2. Upon the addition of H_2O_2 to test solution, the green emission band from the **Np** acceptor at λ_{em} = 525 nm was gradually intensified, accompanied by blue emission weakening. The green emission enhancement is contributed by the ICT-dominated fluorescence of **Cm–Np** and the FRET process from **Cm** to **Np**, while the blue emission decrease is ascribed to the FRET process. Similar to the unchanged UV-vis absorption spectrum with H_2O_2, **Cm–Np-B** showed no fluorescence response to H_2O_2 (Fig. S12, ESI†), corroborating the superior capability of the artificial protein-probe hybrid in H_2O_2 detection. Besides these, the time-dependent fluorescence response of probe-protein hybrid **Cm–Np-B@BSA** and **Cm–Np-B** toward H_2O_2 in PBS buffer was also measured (Fig. S13, ESI†), and **Cm–Np-B@BSA** showed a faster response than **Cm–Np-B**.

The blue-to-green fluorescence emission change in **Cm–Np-B@BSA** enables ratiometric fluorescence detection of H_2O_2 in PBS buffer. As shown in Fig. 2B, the dose-dependent fluorescence response (F_{525}/F_{460}) of **Cm–Np-B@BSA** exhibited a good linearity against the concentration of H_2O_2 in the range of 0–160 μM. The detection limit ($3\sigma/k$) was calculated to be 1 μM. The low detection limit and broad detection range indicate the high sensitivity of artificial protein-probe hybrid **Cm–Np-B@BSA** for H_2O_2 detection.

The selectivity of **Cm–Np-B@BSA** towards H_2O_2 over other interfering species, including some other ROS, anions, and biomolecules, was also confirmed. **Cm–Np-B@BSA** in PBS buffer was treated with 200 μM of H_2O_2 and 500 μM of other species, respectively. After 10 min incubation, remarkable changes of the fluorescence of **Cm–Np-B@BSA** were noticed in the presence of H_2O_2, but not in the presence of other species ($F_{525/460}$, Fig. S14, ESI†). Furthermore, the competitive selectivity of **Cm–Np-B@BSA** to H_2O_2 over other species was also tested. As shown in Fig. S15 (ESI†), the fluorescence ($F_{525/460}$) was increased exclusively to H_2O_2 and the enhancement of fluorescence intensity was not affected in the presence of all competitive species. These data indicate the high selectivity of protein-probe hybrid **Cm–Np-B@BSA** for a ratiometric fluorescence response to H_2O_2 in PBS buffer.

Then, the effect of pH on the ratiometric fluorescence response of **Cm–Np-B@BSA** to H_2O_2 was examined in PBS buffer with pH 5–8. As shown in Fig. S16E (ESI†), no obvious difference in the emission spectra was observed in solutions with pH 6–8, suggesting that the **Cm–Np-B@BSA** probe is able to detect H_2O_2 in an environment with pH 6–8, while the peak at 525 nm in pH 5 solution was relatively weaker, probably due to the acidity slowing down the H_2O_2 detection reaction.

Encouraged by the excellent sensitivity and selectivity of the **Cm–Np-B@BSA** response to H_2O_2, we further demonstrated the application of this artificial protein-probe hybrid for imaging H_2O_2 in living cells. MTT assay showed that **Cm–Np-B@BSA** had low cytotoxicity towards RAW 264.7 macrophage cells (Fig. S17, ESI†). For example, the cell viability remained over 85% after incubation of RAW 264.7 macrophage cells with **Cm–Np-B@BSA** (60 μM/50 μM) for 24 h. For safety, 5 μM/50 μM of **Cm–Np-B@BSA** was used in most subsequent experiments.

The capability of **Cm–Np-B@BSA** in visualizing intracellular H_2O_2 in RAW 264.7 cells was then examined. As shown in Fig. 3A, clear blue fluorescence was noticed after incubating RAW 264.7 cells with **Cm–Np-B@BSA** for 2 h, which was remarkably increased in comparison with the control group (RAW 264.7 macrophage cells only) (Fig. S18, ESI†). The flow cytometric data showed a similar change. Both observations confirm the effective cell internalization of **Cm–Np-B@BSA** (Fig. S19, ESI†). Interestingly, supplying **Cm–Np-B@BSA**-internalized cells with H_2O_2 (200 μM), the intracellular blue channel fluorescence was largely quenched, while intense green channel fluorescence emerged (Fig. 3A). This remarkable change was also confirmed by flow cytometric analysis (Fig. 3B), in agreement with spectrometric
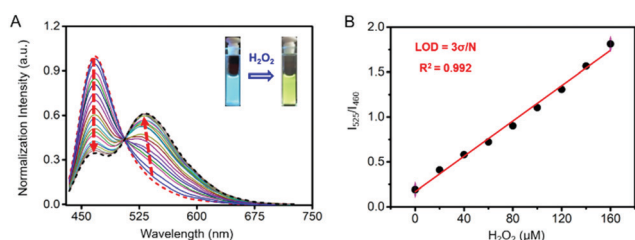
Fig. 2 Sensitivity and selectivity of **Cm–Np-B@BSA** (5/50 μM) for H_2O_2 detection. (A) Fluorescence spectral response of **Cm–Np-B@BSA** (5/50 μM) to H_2O_2 at the concentration of 0–200 μM; (B) linear detection range and limit of detection (LOD) of **Cm–Np-B@BSA** (5/50 μM). All measurements were carried out in PBS buffer, pH 7.4, excitation wavelength: 410 nm.
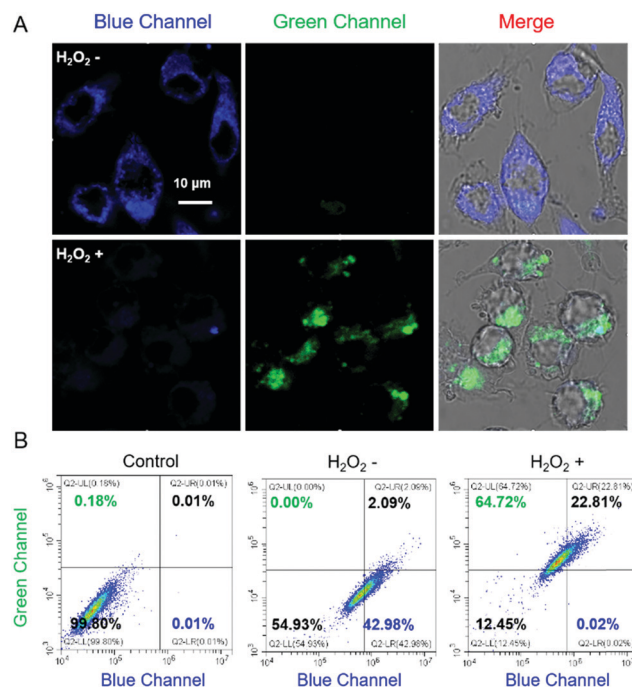
Fig. 3 Fluorescence imaging and flow cytometric data of Raw 264.7 cells using **Cm–Np-B@BSA** (5/50 μM) as the probe. (A) Fluorescence imaging of living cells with (H_2O_2+) or without (H_2O_2−) exogenous H_2O_2 (200 μM); (B) flow cytometric data of cells with (H_2O_2+) or without (H_2O_2−) exogenous H_2O_2 (200 μM). λ_{ex} = 405 nm, λ_{em} = 460–480 and 520–560 nm for blue and green channels, respectively. The images were recorded by confocal laser-scanning microscopy (scale bar = 10 μm).

5422 | *J. Mater. Chem. B*, 2020, **8**, 5420–5424

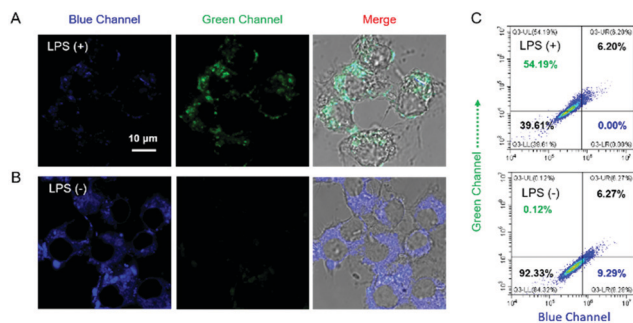This journal is © The Royal Society of Chemistry 2020

Fig. 4 Fluorescence imaging of Raw 264.7 cells pretreated with LPS using **Cm–Np-B@BSA** (5/50 μM) as the probe. (A) Fluorescence imaging of living cells pretreated with 80 ng mL^{-1} of LPS; (B) control group of cells; (C) flow cytometric data of Raw 264.7 cells. λ_{ex} = 405 nm, λ_{em} = 460–480 and 520–560 nm for blue and green channels, respectively. The images were visualized by confocal laser-scanning microscopy (scale bar = 10 μm).

analysis (Fig. 2A) and in sharp contrast to that using **Cm–Np-B** for the same fluorescence imaging and flow cytometric analysis, where only small alternation in the fluorescence blue and green channels was observed (Fig. S20, ESI†). Thus the sharp contrast corroborates the high sensitivity of the fluorescent protein-probe hybrid (**Cm–Np-B@BSA**) for intracellular H_2O_2 detection.

The capability of **Cm–Np-B@BSA** for ratiometric fluorescence visualization of intracellular H_2O_2 generation was further evaluated in LPS-stimulated RAW 264.7 macrophage cells. As shown in Fig. 4, obvious fluorescence emissions in both the blue and green channels were observed, suggesting that **Cm–Np-B@BSA** is able to detect endogenous H_2O_2 in live cells.

In summary, we developed an artificial protein-probe hybrid, **Cm–Np-B@BSA**, for ratiometric fluorescence detection and imaging of H_2O_2 in physiological buffers and live cells. **Cm–Np-B@BSA** was devised by assembling H_2O_2-responsive **Cm–Np-B** molecules with BSA *via* host–guest interactions. The strong binding of **Cm–Np-B** with BSA occurred at the preferred site I of BSA. In this complex, blue channel emission (λ_{em} = 460 nm) was activated (>145-fold enhancement) while the green channel (λ_{em} = 525 nm) remained weakly fluorescent. Cleavage of a borate group of **Cm–Np-B@BSA** by the H_2O_2-initialized reaction generated a new product **Cm–Np@BSA**, and enabled green channel emission observable as the result of FRET from Cm to Np. This change allowed **Cm–Np-B@BSA** to be used in ratiometric fluorescence detection of H_2O_2 in aqueous solution. This **Cm–Np-B@BSA** exhibited high sensitivity and selectivity for H_2O_2 detection with good biocompatibility, and demonstrated ratiometric fluorescence detection of H_2O_2 in live macrophage cells. Thus, the success in developing **Cm–Np-B@BSA** not only provides a useful tool to monitor H_2O_2 generation in live cells, but also offers a feasible way to design new artificial protein-probe hybrids for biomolecule detection and imaging.

Conflicts of interest

There are no conflicts to declare.

Acknowledgements

Notes and references

1 A. Miyawaki and Y. Niino, *Mol. Cell*, 2015, **58**, 632–643.
2 H. Zhu, J. Fan, J. Du and X. Peng, *Acc. Chem. Res.*, 2016, **49**, 2115–2126.
3 E. A. Rodriguez, R. E. Campbell, J. Y. Lin, M. Z. Lin, A. Miyawaki, A. E. Palmer, X. Shu, J. Zhang and R. Y. Tsien, *Trends Biochem. Sci.*, 2017, **42**, 111–129.
4 E. Eroglu, S. Charoensin, H. Bischof, J. Ramadani, B. Gottschalk, M. R. Depaoli, M. Waldeck-Weiermair, W. F. Graier and R. Malli, *Free Radical Biol. Med.*, 2018, **128**, 50–58.
5 Z.-j. Chen and H.-w. Ai, *Biochemistry*, 2014, **53**, 5966–5974.
6 S. Sun, Y. Liu, J. Xia, M. Wang, R. Tang, C. Lei, Y. Huang, Z. Nie and S. Yao, *Chem. Commun.*, 2019, **55**, 2218–2221.
7 K. Fukunaga, T. Watanabe, D. Novitasari, H. Ohashi, R. Abe and T. Hohsaka, *Chem. Commun.*, 2018, **54**, 12734–12737.
8 D. M. Chudakov, M. V. Matz, S. Lukyanov and K. A. Lukyanov, *Physiol. Rev.*, 2010, **90**, 1103–1163.
9 H. Shinoda, M. Shannon and T. Nagai, *Int. J. Mol. Med.*, 2018, **19**, 1548.
10 X. Liu, Z. Ye, W. Wei, Y. Du, J. Yuan and D. Ma, *Chem. Commun.*, 2011, **47**, 8139–8141.
11 L. Tian, Z. Dai, X. Liu, B. Song, Z. Ye and J. Yuan, *Anal. Chem.*, 2015, **87**, 10878–10885.
12 J. Du, T. Zhu, Q. Gu, W. Cao, J. Fan and X. Peng, *Sens. Actuators, B*, 2018, **263**, 661–667.
13 S. Yoo and M. S. Han, *Chem. Commun.*, 2019, **55**, 14574–14577.
14 Y. Fu, H.-H. Han, J. Zhang, X.-P. He, B. L. Feringa and H. Tian, *J. Am. Chem. Soc.*, 2018, **140**, 8671–8674.
15 R. Zhang, B. Song and J. Yuan, *TrAC, Trends Anal. Chem.*, 2018, **99**, 1–33.
16 R. Sindhu, A. K. Tiwari, L. C. Mishra and M. M. Husain, *Cancer Biother. Radiopharm.*, 2012, **27**, 452–456.
17 T. Bayraktutan and Y. Onganer, *Dyes Pigm.*, 2017, **142**, 62–68.
18 S. C. Kampranis, N. A. Gormley, R. Tranter, G. Orphanides and A. Maxwell, *Biochemistry*, 1999, **38**, 1967–1976.
19 S. I. Reja, I. A. Khan, V. Bhalla and M. Kumar, *Chem. Commun.*, 2016, **52**, 1182–1185.
20 J. Park and Y. Kim, *ChemBioChem*, 2019, **20**, 350–354.
21 H. H. Han, A. C. Sedgwick, Y. Shang, N. Li, T. Liu, B. H. Li, K. Q. Yu, Y. Zang, J. T. Brewster, M. L. Odyniec, M. Weber, S. D. Bull, J. Li, J. L. Sessler, T. D. James, X. P. He and H. Tian, *Chem. Sci.*, 2020, **11**, 1107–1113.
22 H. Xiao, P. Li, S. Zhang, W. Zhang, W. Zhang and B. Tang, *Chem. Commun.*, 2016, **52**, 12741–12744.

This journal is © The Royal Society of Chemistry 2020

J. Mater. Chem. B, 2020, **8**, 5420–5424 | **5423**

23 H. Xiao, P. Li, X. Hu, X. Shi, W. Zhang and B. Tang, *Chem. Sci.*, 2016, **7**, 6153–6159.

24 Y. Chen, X. Shi, Z. Lu, X. Wang and Z. Wang, *Anal. Chem.*, 2017, **89**, 5278–5284.

25 H. Wang, Z. He, Y. Yang, J. Zhang, W. Zhang, W. Zhang, P. Li and B. Tang, *Chem. Sci.*, 2019, **10**, 10876–10880.

26 L. Chen, S. Xu, W. Li, T. Ren, L. Yuan, S. Zhang and X.-B. Zhang, *Chem. Sci.*, 2019, **10**, 9351–9357.

27 W. Zhang, J. Zhang, P. Li, J. Liu, D. Su and B. Tang, *Chem. Sci.*, 2019, **10**, 879–883.

28 W. Gao, Y. Zhao, X. Li, Y. Sun, M. Cai, W. Cao, Z. Liu, L. Tong, G. Cui and B. Tang, *Chem. Sci.*, 2018, **9**, 439–445.

29 T. F. Brewer, F. J. Garcia, C. S. Onak, K. S. Carroll and C. J. Chang, *Annu. Rev. Biochem.*, 2015, **84**, 765–790.

30 Y. Hitomi, T. Takeyasu and M. Kodera, *Chem. Commun.*, 2013, **49**, 9929–9931.

31 J. Zhang, L. Shi, Z. Li, D. Li, X. Tian and C. Zhang, *Analyst*, 2019, **144**, 3643–3648.

32 M. Abo, Y. Urano, K. Hanaoka, T. Terai, T. Komatsu and T. Nagano, *J. Am. Chem. Soc.*, 2011, **133**, 10629–10637.

33 Y. Liu, C. Jiao, W. Lu, P. Zhang and Y. Wang, *RSC Adv.*, 2019, **9**, 18027–18041.

34 X. Chen, X. Tian, I. Shin and J. Yoon, *Chem. Soc. Rev.*, 2011, **40**, 4783–4804.

35 S. Banerjee, E. B. Veale, C. M. Phelan, S. A. Murphy, G. M. Tocci, L. J. Gillespie, D. O. Frimannsson, J. M. Kelly and T. Gunnlaugsson, *Chem. Soc. Rev.*, 2013, **42**, 1601–1618.

36 V. Marx, *Nat. Methods*, 2017, **14**, 949.

37 X. Liang, X. Xu, D. Qiao, Z. Yin and L. Shang, *Chem. – Asian J.*, 2017, **12**, 3187–3194.

38 C. Yik-Sham Chung, G. A. Timblin, K. Saijo and C. J. Chang, *J. Am. Chem. Soc.*, 2018, **140**, 6109–6121.

39 X. Ma, R. Sun, J. Cheng, J. Liu, F. Gou, H. Xiang and X. Zhou, *J. Chem. Educ.*, 2016, **93**, 345–350.

40 S. Patra, K. Santhosh, A. Pabbathi and A. Samanta, *RSC Adv.*, 2012, **2**, 6079–6086.

41 M. S. Baptista and G. L. Indig, *J. Phys. Chem. B*, 1998, **102**, 4678–4688.

42 X. Cao, Y. He, D. Liu, Y. He, X. Hou, Y. Cheng and J. Liu, *RSC Adv.*, 2018, **8**, 25519–25525.

5424 | *J. Mater. Chem. B*, 2020, **8**, 5420–5424

This journal is © The Royal Society of Chemistry 2020